Coastal Erosion from Space

Coastal Erosion events:

in Nerja (Spain) in Kilkee (Ireland) in St Laurent mouth (Canada)

Algorithm Theoretical Baseline Document

Ref: SO-TR-ARG-003-055-009-ATBD-WL

Date: 03/12/2019

Customer: ESA

Contract Ref.: ESA/AO/1-8758/16/NL/PSI-LG

This page is intentionally left blank

Version and Signatures

Version	Date	Modification
Written by: Albert Garcia-Mondéjar (isardSAT)	29/08/2019	Template
	02/10/2019	First version
	21/11/2019	Review
	03/12/2019	Modifications according to revision
Verification by		
Authorisation by:		

Acronyms

ALOS	Advanced Land Observation Satellite
AMI	Active Microwave Instrument
CSI	Coastal State Indicators
CSK	COSMO-SkyMed
EO	Earth Observation
ERS	European Remote Sensing satellite
EWS	Extra Wide Swath
GDR	Ground Range Detected
IW	Interferometric Wide Swath
PSI	Persistent Scatterer Interferometry
RCM	RADARSAT Constellation Mission
ROI	Region of interest
S1	Sentinel 1
SAR	Synthetic Aperture Radar
SC	ScanSAR
SCW	ScanSAR Wide Swath
SI	Shoreline Indicators
SL	SpotLight
SM	Strip Map
SNR	Signal to noise ratio
WL	Waterline
WM	Wide Mode

Applicable and reference documents

Id	Description	Reference
AD-1	Requirement Baseline Document	SO-RP-ARG-003-055-006-RBD_v1.0_20190916

Contents

List of Figures

List of Tables

1 Overview and Background Information

1.1 Product requirement

The overall objective of the Coastal Erosion from Space project is to retrieve Coastal State Indicators (CSI) which describe the dynamic-state and evolutionary trends of coastal systems, from Shoreline Indicators (SI), gauges, pointers or markers that are used as proxies to represent the shore (either visible discernible features, or tidal datum-based indicators) to get isobaths and isohypses (contour lines).

Coast, coastline, shore and shorelines are often confused, although the focus on the same geographical features:

- a shore or a shoreline is the fringe of land at the edge of a body of water (the ‘line’ is quite thick on a large-scale map, e.g. 1: 5,000, but very thin on a small scale map, e.g. 1: 1,000,000. Thus, a precise line that can be called a shoreline cannot be determined if it does not refer to a representation scale or spatial frequency cut),
- a coast, also called coastline or seashore, is a shore which borders the sea; however, coast often refers to an area far wider than the shore, often stretching miles into the hinterland.

1.1.1 Information content quality and value

1D EO products, shorelines from waterlines, are designed by identifying points in the digital images at which the image characteristics change sharply when coming landward from the sea. Those shorelines are needed to map and study the dynamics of the land/water interface whether visible or not to the human eye.

Land/water delimitation is generally equated with the maritime boundary; however, all land/water edges are not necessarily maritime. We have the example of lacs, riverbanks or offshore sand bars that may be underwater most of the time. We here consider as waterline, each land/water interface connected to the sea and inside our "coastal area", i.e. buffer around the coast which delimits our area of interest for the project. We thus consider riverbanks near the coast if it's open to the sea, and offshore sand bars when they are above water.

1.1.2 Product order & delivery services

The 1D proxy-based shoreline indicator (waterline) product will be based on the following EO data for a 25-year period:

- use of different spectral properties of SAR data sets as reported in studies exploiting data at different resolutions[1] (ERS and Envisat at 30 meters, Sentinel 1A and Sentinel 1B 5 meters).

With the following formatting:

CE_ISR_*area*_L2_1D_OB_WL_*mission_date-hour*.shp
being

CE	Coastal Erosion
ISR	isardSAT
area	the area to be processed: specific pilot area, country
WL	WaterLine
Mission	ERS/ENV/S1A/S1B

It may evolve in next version

Delivery as an ESRI shapefile for GIS software.

1.2 Quick Review – Feasibility

At the state of the art (Mason and Davenport, 1996; Lee and Jurkevich, 1990) several research studies have been performed for the extraction of the coastline from remotely sensed images. Most of them exploit methodologies and algorithms related to the grey-level feature of the images concerned. This is not always useful when considering SAR images because the sea is generally not characterised by uniform grey levels.

1.2.1 Satellite sensors and mission

The below table contains the most significant SAR missions that could provide EO products as inputs for shoreline studies. It refers to the geometric ground resolution of the sensors, the resolution of images that are delivered by the satellite operators, and the point spread function (PSF) which is the "true" resolution of an image; these three parameters are seldom supplied concurrently, and images

[1] Resolution of the sensor without any multilooking and in Stripmap acquisition mode.

are the result of a gridding of the measurements, with pixels that may be smaller than the resolution of the sensors; as such the resolution of the image does not inform exactly on the information content scale of the image.

Satellite constellation	Sensor modes	pixel resolution of L1 products	Revisit time	Years active
ERS1 ERS2 (C-band)	AMI	<30 m x <26.3 m	35 days	1991-2000 1995-2003
Envisat/ASAR (C-band)	Image Mode Wide Swath Mode Alternating/Cross Polarization Wave Mode Global Monitoring	28 m x 28 m 150 m x 150 m 29 m x 30 m 28 m x 30 m 950 m x 980 m	35 days	2004-2012
Sentinel-1A Sentinel 1B (C-band)	SM IWS EWS WM	5 m x 5 m 5 m x 20 m 25 m x 80 m 20 m x 5 m	6 days	S1A 2014- S1B 2016-
Radarsat 1 (C-band)	Standard Wide (1) Wide (2) Fine Resolution ScanSAR (N) ScanSAR (W)	25 x 28 40 x 28 40 x 28 10 x 9 50 x 50 100x100	4 days, exact revisit every 24 days	1995-2010
Radarsat 2 (C-band)	Wide ultrafine Wide multi-look fine Wide fine Wide fine Quad-Pol Wide standard Quad-Pol	1.6 - 3.3 x 2.8 m^2 3.1-10.4 x 4.6-7.6 m^2 5.2-15.2 x 7.7 m^2 5.2-17.3 x 7.6 m^2 9-30.0 x7.6 m^2	4 days, exact revisit every 24 days	2007-
RCM (C-band) 3 satellite constellation	Low Res Med Res 50 Med Res 16 Med Res 30 High Res 5 Very High Res Low Noise Spotlight	100 x 100 50 x 50 30 x 5 3 x 3 4 x 2 1 x 3	daily, exact revisit every 4 days	June/2019-
ALOS (L-Band)	Stripmap fine ScanSAR Polarimetric	7 m 100 m 24 m	14 days	2006 – 2011
ALOS 2 (L-Band)	Stripmap Ultrafine Stripmap High sensitive Stripmap fine ScanSAR Normal ScanSAR Wide Spotlight	3 m 6 m 10 m 100 m 60 m 3 m	14 days	2014 -
SAOCOM 1A SAOCOM 1B (L-band)	Stripmap TopSAR narrow TopSAR wide	< 10 m < 30-50 m < 50-100	Daily	October/2018 - February/2020 -
NovaSAR (S-band)	Stripmap Stripmap (wide swath) Stripmap x-polarization Maritime (ScanSAR) ScanSAR Dual polarization Tri polarization	6 x 6 m^2 6 x 6 m^2 6 x 10 m^2 6 x 14 m^2 20 x 20 m^2 20 x 20 m^2 30 x 35 m^2	0.4 days for ScanSAR, 0.3 days for Stripmap and ScanSAR Wide and 0.2 days for Maritime Surveillance	September/2018 -

Cosmos-SkyMed 1 Cosmos-SkyMed 2 Cosmos-SkyMed 3 Cosmos-SkyMed 4 (X-band)	Spotlight ("Frame") HIMAGE (Stripmap) WideRegion (ScanSAR) HugeRegion (ScanSAR) Ping Pong (Stripmap)	< 1m 3-15 m 30 m 100 m 15 m	16 days	June/2007 - December/2007 - October/2008 - November/2010 -
TerraSAR-X Tandem X (X-band)	ScanSAR Wide (SCW) ScanSAR (SC) Stripmap (SM) Spotlight (SL) High-Resolution Spotlight (HS) Sliding Spotlight (HS) Staring Spotlight (ST)	40 m 18 m 3 m 1.7 m - 3.5 m 1.4 m - 3.5 m 1.1 m – 1.8 m 0.9 m – 1.8 m	11 days	2008 - 2010 -
COSMO-SkyMed Second Generation	Spotlight-2A Spotlight-2B Stripmap Pingpong Quadpol ScanSAR-1 ScanSAR-2	0.35 x 0.48/0.55 m^2 0.63 x 0.63 m^2 3 x 3 m^2 12 x 5 m^2 3 x 3 m^2 20 x 4 m^2 40 x 6 m^2	Hourly with full constellation	17/12/2019 - (scheduled)
PAZ (X-band)	Stripmap ScanSAR Spotlight HR Spotlight	3 m x 3 m 6 m x 6 m 16 m x 6 m 1 m x 1 m 2 m x 2 m < (1 m x 1 m) < (2 m x 2 m)	11 days	2018 -
ICEYE X1 ICEYE X2 ICEYE X3 ICEYE X4 ICEYE X5 (X-Band)	Stripmap Stripmap Hig ScanSAR Spotlight	3 m x 3 m 1.5 m x 1.5 m 20 m x 20 m 1 m x 1 m	3 hour with 18 satellites	January/2018- December/2018- May/2019- July/2019 - July/2019 -
Capella X-SAR (X-Band)	Spotlight Sliding Spotlight Stripmap Multi-swath Stripmap	0.3 x 0.5 m 0.018 x 0.5 m 0.3 x 0.3 m 0.3 x 0.3 m	Weekly with 2 satellites, Hourly with full constellation, 36 satellites	December/2018 -

The pixel resolution is linked to the bandwidth (range) and the antenna along track length (azimuth). For a specific SAR instrument, the Strip map mode is associated with the nominal resolution. The conventional SAR strip mapping mode assumes a fixed pointing direction of the radar antenna broadside to the platform track. HR SAR products are linked to Spotlight acquisition mode. It obtains high-resolution by steering the radar beam to keep the target within the beam for a longer time and thus form a longer synthetic aperture whereas in the ScanSAR the resolutions are usually the worse as it aims to improve the coverage by illuminating several sub-swaths, scanning its antenna off-nadir into different positions.

1.2.2 Models specification [2]

Lee and Jurkevich [3] (1990) were among the first who detected the shoreline using SAR imagery. They proposed a shoreline extraction technique based on Sobel edge detection for a small portion of a SEASAT image. Mason and Davenport [4] (1996) employed a coarse-fine resolution processing approach to extract the shoreline. In their approach, the sea regions were firstly detected as regions of low edge density in a low resolution image. Then the area of the image near the shoreline is subjected to more elaborate processing at high resolution using an active contour model. Liu and Jezek[5] (2004) developed an effective approach for shoreline extraction integrated by Canny edge detection and an image segmentation based on a locally adaptive thresholding technique. Shu, Li, and Gomes[6] (2010) presented a semi-automated method for shoreline extraction from Radarsat-2 imagery. They used a morphological filtering to segment the SAR image into the land and the sea. Then a narrow band level segmentation was implemented to refine the segmentation and thus determine the shoreline.

---

[2] Lianhui Wu, Yoshimitsu Tajima, Yusuke Yamanaka, Takenori Shimozono & Shinji Sato (2019) Study on characteristics of SAR imagery around the coast for shoreline detection, Coastal Engineering Journal, 61:2, 152-170, DOI: 10.1080/21664250.2018.1560685

[3] Lee, J. S., and I. Jurkevich. 1990. "Coastline Detection and Tracing in SAR Images." IEEE Transactions on Geoscience and Remote Sensing 28 (4): 662–668. doi:10.1109/TGRS.1990.572976.

[4] Mason, D. C., and I. J. Davenport. 1996. "Accurate and Efficient Determination of the Shoreline in ERS-1 SAR Images." IEEE Transactions on Geoscience and Remote Sensing 34 (5): 1243–1253. doi:10.1109/36.536540.

[5] Liu, H., and K. C. Jezek. 2004. "Automated Extraction of Coastline from Satellite Imagery by Integration Canny Edgy Detection and Local Adaptive Thresholding Methods." International Journal of Remote Sensing 25 (5): 937–958. doi:10.1080/0143116031000139890.

[6] Shu, Y., J. Li, and G. Gomes. 2010. "Shoreline Extraction from RADARSAT-2 Intensity Imagery Using a Narrow Band Level Set Segmentation Approach." Journal of Geodesy 33 (2–3): 187–203. doi:10.1080/01490419.2010.496681.

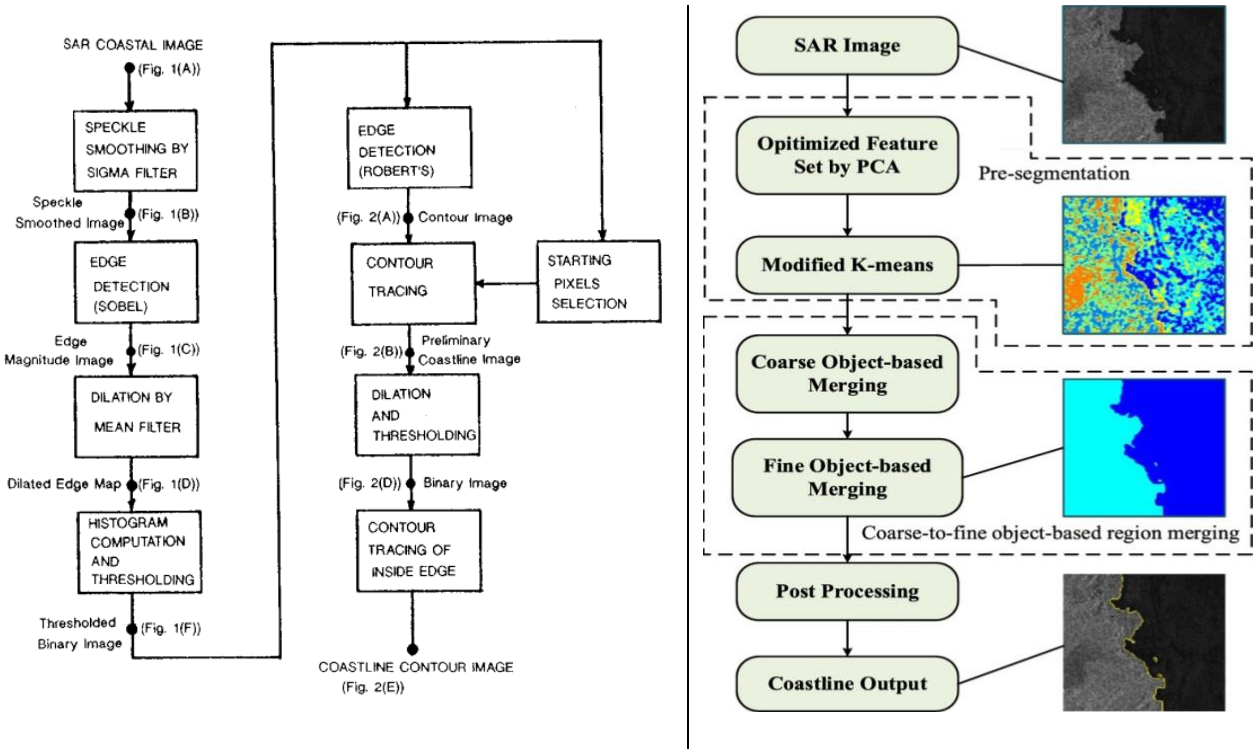

Figure 1 left: Block diagram of coastline detection and training in Lee and Jurkevich (1990) right: Flowchart of the proposed method "MKAORM" in Liu, Z. et al. (2016)

Paes, Nunziata, and Miliaccio[7] (2015) proposed a method for shoreline detection from Radarsat-2 SAR data by using k-means clustering algorithm and Canny edge detection filter. Liu et al.[8] (2016) presented a method for shoreline extraction for the wide-swath SAR imagery. The method used the modified k-means method and an adaptive coarse-fine object-based region-merging (MKAORM) which reduces the high computation cost for shoreline extraction from wide-swath SAR imagery without losing the accuracy.

[7] Paes, R. L., F. Nunziata, and M. Migliaccio. 2015. "Coastline Extraction and Coastal Area Classification via SAR Hybridpolarimetry Architecture." Paper presented at IEEE International Geoscience and Remote Sensing Symposium (IGARSS), Milan, July. 3798–3801. doi: 10.1109/IGARSS.2015.7326651.

[8] Liu, Z., F. Li, N. Li, R. Wang, and H. Zhang. 2016. "A Novel Region-Merging Approach for Coastline Extraction from Sentinel-1A IW Mode SAR Imagery." IEEE Geoscience and Remote Sensing Letters 13 (3): 324–328. doi:10.1109/LGRS.2015.2510745.

Modava and Akbarizadeh[9] (2017) utilized a fuzzy clustering with spatial constraints on SAR images and then extracted the shoreline by an active contour model. The method was robust against noise and showed good performance especially in noisy images.

Although many image processing techniques have been developed for shoreline extraction based on SAR imagery, it is not fully understood to what extent the signal returned from the sea surface differs from that from the neighbouring land surface. his fundamental but most essential problem is one of the key factors for detection of the land-sea boundary since most of shoreline detection technique relies on such difference of the returned signal from the land and the sea. The contrast between the land and the sea is significantly affected by many parameters such as polarization method, land morphology, sea surface conditions, and incident angle of the radar. Rijkswaterstaat[10] (2006) indicated that the differences of polarimetric channels are less useful to separate the land from the sea than the channels themselves, and HH (horizontal transmit and horizontal receive) is the most preferred polarization mode for shoreline detection. Incident angles preferred for shoreline detection should be either small (near 15°) or large (near 45°) depending on the roughness of the land surface. Their conclusions, however, are mostly based on theoretical analysis rather than the direct analysis of the real SAR data. Kim et al.[11] (2007) investigated the shoreline mapping in the intertidal areas using airborne L- and P-band SAR scenes. They suggested that the radar with shorter wavelength is preferred for better shoreline mapping over the gently sloping beaches because the Bragg waves resonant with different frequencies reside in different regions. Vandebroek et al.[12] (2017) studied the capability of shoreline monitoring of a mega-scale beach nourishment and the

---

[9] Modava, M., and G. Akbarizadeh. 2017. "Coastline Extraction from SAR Images Using Spatial Fuzzy Clustering and the Active Contour Method." International Journal of Remote Sensing 38 (2): 355–370. doi:10.1080/01431161.2016.1266104.

[10] Rijkswaterstaat. 2006. Land Water Detection with Polarimetric SAR, 1–67. Netherland: Ministry of Infrastructure and the Environment.

[11] Kim, D., W. M. Moon, S. Park, J. Kim, and H. Lee. 2007. "Dependence of Waterline Mapping on Radar Frequency Used for SAR Images in Intertidal Areas." IEEE Geoscience and Remote Sensing Letters 4 (2): 269–273. doi:10.1109/LGRS.2006.888843.

[12] Vandebroek, E., R. Lindenbergh, F. van Leijen, M. de Schipper, S. de Vries, and R. Hanssen. 2017. "Semi-Automated Monitoring of a Mega-Scale Beach Nourishment Using High-Resolution TerraSAR-X Satellite Data." Remote Sensing 9 (7): 653. doi:10.3390/rs9070653.

influence of environmental conditions on such monitoring skills. They found that large waves have a significant effect on shoreline detection, while rainfall and temperature have a relatively minor influence. They also indicated that the shallower incident angle (39°) is much better than the steeper incident angle and this conclusion contradicts that presented by Rijkswaterstaat (2006).

Most of these existing studies are based on limited number of SAR scenes and have not fully clarified the overall characteristics of how SAR-based shoreline detection capabilities depend on SAR parameters and other environmental conditions. Understanding such characteristics is essential for the selection of optimum imagery configuration for shoreline detection at each target site. Motivated by the discussion in the above, this study conducts a comprehensive analysis of the characteristics of SAR imagery around the coast with different SAR parameters and natural conditions. We also evaluate the effect of these factors on SAR-imagery-based shoreline detection.

1.2.3 Auxiliary data

To improve the accuracy and relevance of the EO data, the correction of the derived proxy shorelines for astronomical tides is necessary. Tides pose a crucial influence on the instantaneous waterlines, especially considering how much tidal ranges differ around the world. Although the prediction of astronomical tides is fairly straightforward, meteorological conditions and sea state significantly alter where the waterline is at any given instant on a beach. Therefore, any EO-based proxy shoreline needs to be corrected for and/or accompanied by accurate tidal and metocean data.

The computation of EO-based waterlines could benefit from the addition of approximate country shorelines/rough coastlines to the process to make it more efficient – e.g. country or coastline shapefiles available from the respective countries' authorities (statistics offices, local government, etc.) or from a library of geospatial data (e.g. ESRI). The coordinate reference systems of the EO products and the auxiliary rough coastline files should be identical.

For local analysis, the option of having corner reflectors to better georeferenced the different image acquisitions could be very beneficial and will allow the use of the PSI technique and perform better deformation analysis. The precise position of these corner reflector will be needed in the analysis.

1.2.4 Currently known issues

Obtaining a continuous waterline from SAR images is not always possible. The radar instruments allow us to obtain images during night and can see through clouds. However, under some circumstances, the retrieval of the waterline cannot be performed.

The currently known issues are:

- Polarisation: Different polarisation acquisition will have different contrast between sea and land areas. Depending on the polarisation of the edge between the two areas would be clearer.

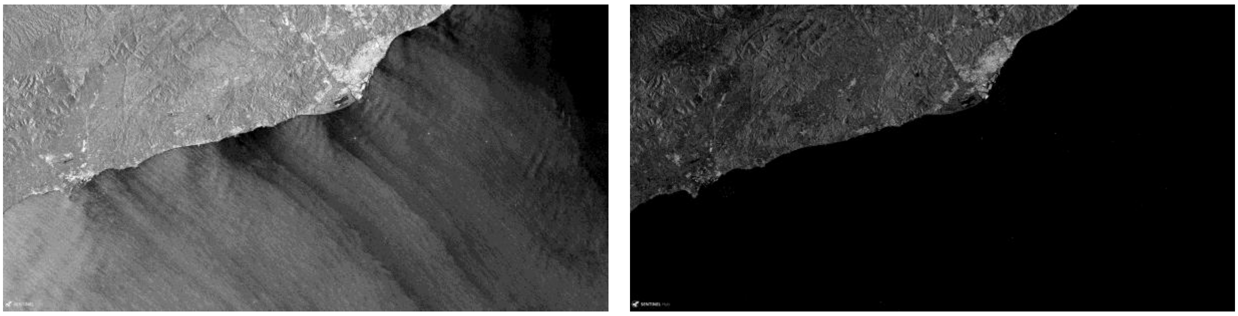

Figure 2. Example of S1 VV acquisition (left) and VH (right) in the coast of Barcelona, 23/11/2019.

- Geometry: Big cliffs shadowing the signal coming from the water at the coast.

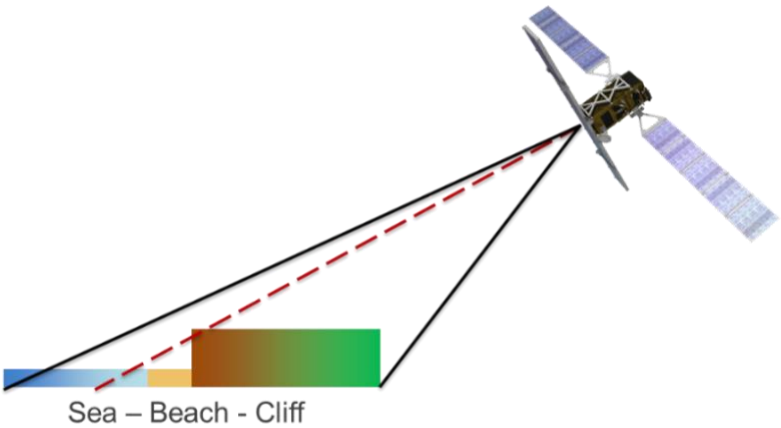

Figure 3. Depiction of an unfavourable Geometry: beaches "hidden" beneath cliffs

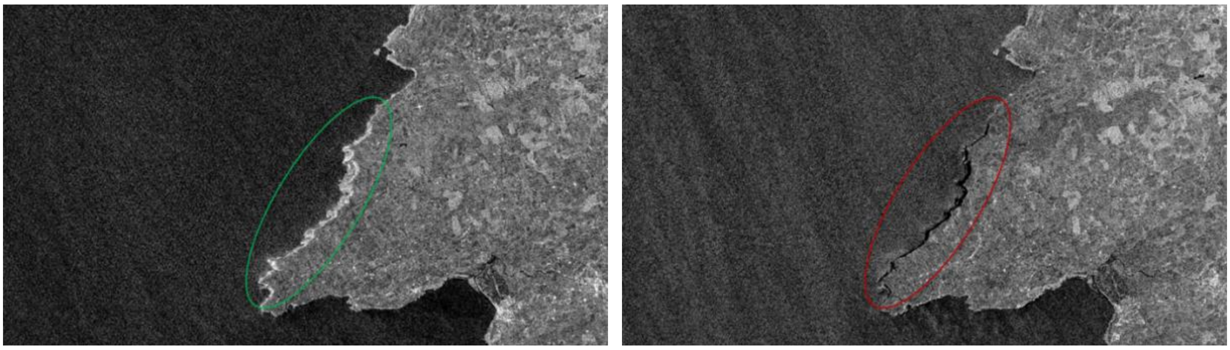

Figure 4. Comparison of Two Sentinel 1 images (left ascending, right descending) over the Cliffs of Moer in the West coast of Ireland. It can be appreciated a dark area in the right image related with the lack of signal coming back to the satellite from that particular area behind the cliff.

- Bright targets (metal structures, vessels, piers …) shadowing the water backscatter.

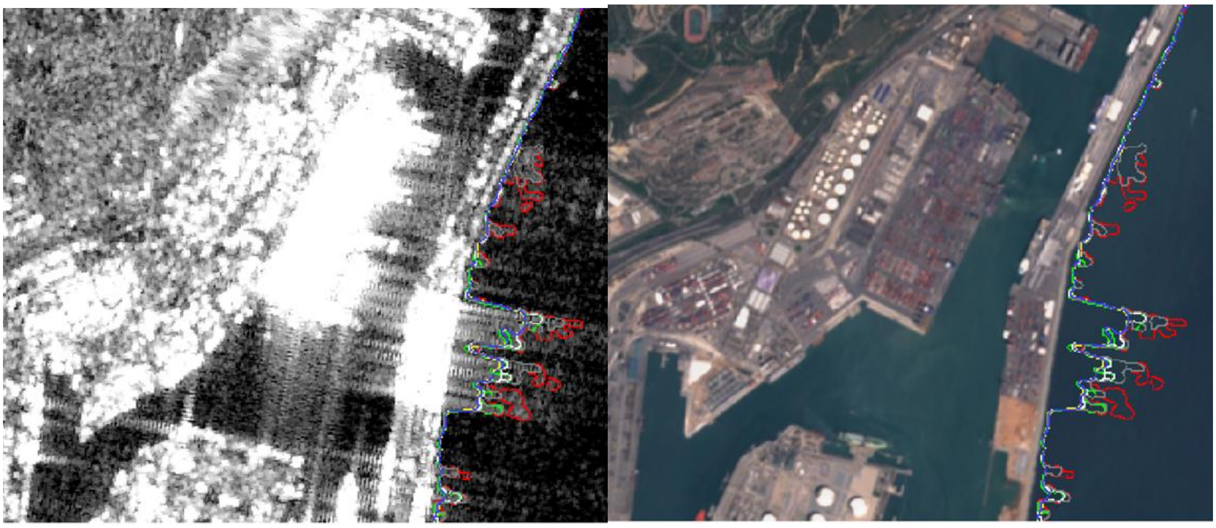

Figure 5. Example of waterline computed in the harbour of Barcelona using different denoisisng methods. It can be appreciated that the metal containers used placed in the surroundings can create bright points in the image that shadow the signal coming from the water next to them.

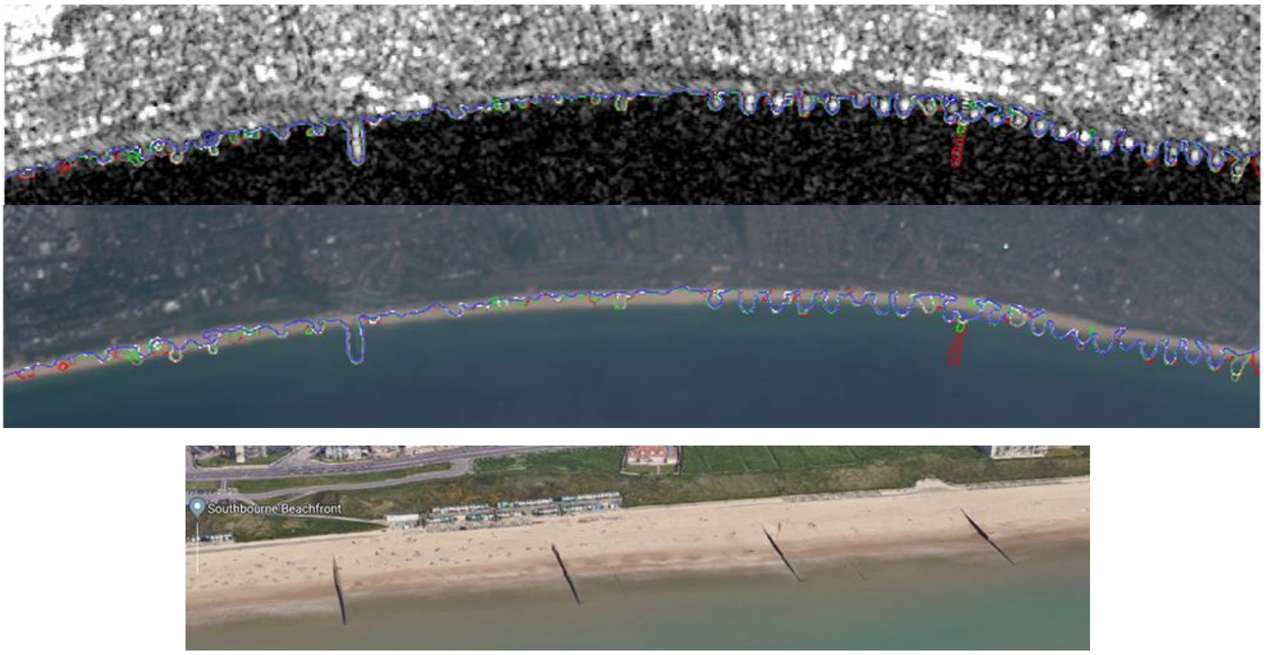

Figure 6. Example of waterline computed in Bournemouth area. It can be appreciated the effect of the sea defences (or groynes) a and piers in the SAR image and the difficulties to retrieve the waterline around them. The waterlines computed with different methods are depicted over a Sentinel 1A (top) and a Sentinel 2A (middle). The bottom image has been extracted from Google Earth to get better details.

- Large waves. In the events with very high waves the sea will become rough instead of a mirroring surface and a lot of signal will be backscattered to the satellite making very difficult to distinguish the boundaries between the water and the land.

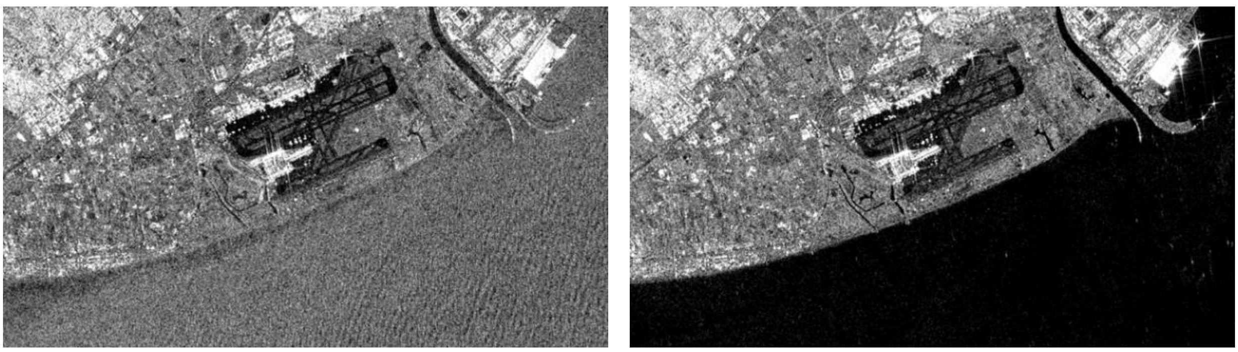

Figure 7. Example of large waves (left) and no waves (right) in the coast of Barcelona, same mode and polarisation, next the airport.

- Penetration of low frequency bands. The grain size of the beach material is relatively fine (0.5 cm) so radars with shorter wavelengths will deliver more accurate measurements of the shoreline.
- Wave breaking area. When the waves are close to the shoreline the start breaking, increasing the roughness and reducing the uniformity of the sea in this particular area. This could be an issue for sensors with small wavelengths.

1.3 Potential Solutions

The HH polarization mode (horizontal transmit and horizontal receive) has been found to be the best mode for shoreline detection on contrast of the backscattering coefficient between the land and sea, the backscattering of active microwave relying on surface[13]roughness and dielectric constant on land, and on Bragg scattering on water, i.e. ripples on the nearshore sea surface—obviously most of the electromagnetic energy of the microwaves is scattered in the same propagation direction and thus the sensor receives relatively stronger backscattering signals in the like-polarization modes; in terms of contrast the backscattering of the land σ_L is higher that the backscattering of the sea σ_S in HH mode whereas σ_S is nearly equal or greater than σ_L in VV mode, σ_L is not sensitive to polarization on bare soils such as silt, sand and gravel, and σ_S (VV) > σ_S (HH); therefore, HH polarization usually generates a larger difference in backscattering between a beach and the sea than that of VV polarization.

SAR scenes with incident angle ranging from 30° to 50° under sea-to-land observation direction are recommended for shoreline detection (incident angles preferred for shoreline detection should be either small or large depending on the roughness of the land surface), with shoreline +/- undetectable if the incident angle is out of the range of these two critical incident angles.

X-band SAR scenes may be preferred to C band, and obviously, L-band SAR scenes for shoreline detection where the grain size of the beach material is relatively fine, while SARs with shorter

[13] without any clear correlation between the significant wave height and the backscattering coefficient of the sea surface; but wave breaking in the nearshore leads to a complex backscattering process and an increase in backscattering coefficient

wavelength also deliver better shoreline mapping over gently sloping beaches because the Bragg waves resonant with different frequencies reside in different regions, but are badly affected by wave breaking.

The use of denoising methods can help to reduce the speckle in the SAR images and provide smoother waterlines. However, it can also over smoothing edges and textures. Denoising filters in combination with anisotropic diffusion is also a valuable option to reduce the speckle in unwanted areas and edges.

1.4 Product Specifications

The shoreline indicator coastline is produced by the addition of in-situ information such as sea state, meteorological forecast, tide information to a waterline which is the instantaneous boundary between water and land. Waterlines will be computed from SAR images using denoising and locally adaptive thresholding methods.

Waterline will be extracted annually or seasonally according to erosion rate to develop regular maintenance works and around storm-event to improve short-term respond and emergency works.

Waterlines will be vectorised and will be available on a geoportal.

2 Algorithm Description

2.1 Data Processing outline

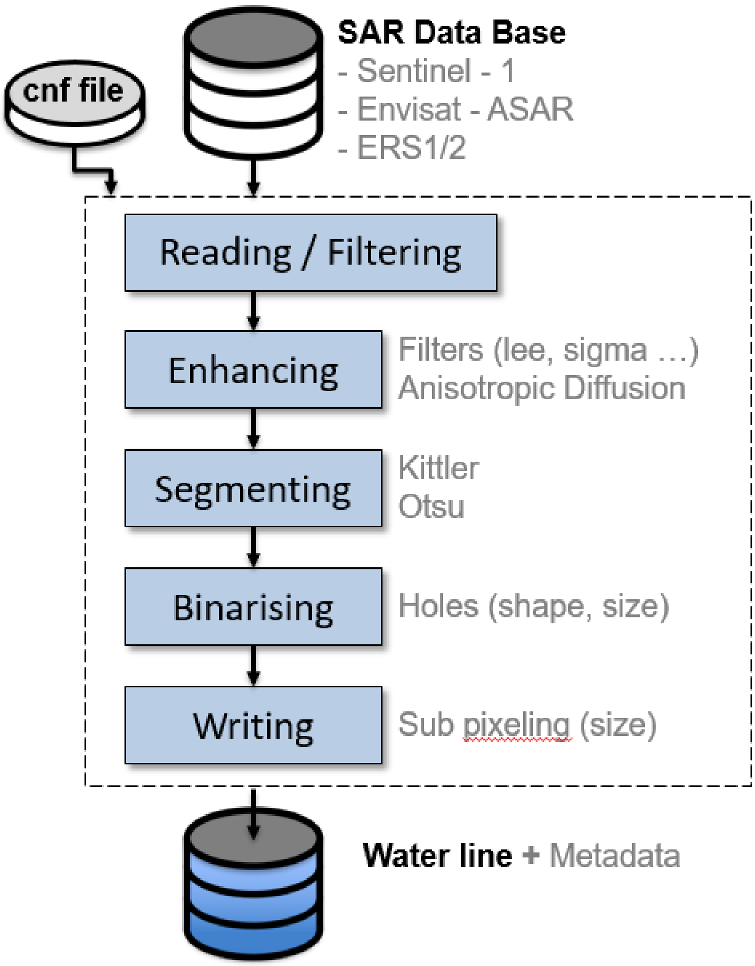

Figure 8. Sketch of the processing chain

The SAR Waterline processor can process different SAR missions. A standardisation step is needed to fit data from different sensor to the right format. A part from the image, some metadata from the headers or auxiliary files is also extracted to be used during the processing.

The SAR waterline processor is in charge of computing the vector line that separates the sea and the land for every input SAR image. The processing chain consists of four main processes: Enhancement, Segmentation, Healing, and Vectorisation. Each of these processes implements a range of options, and are configurable by a range of parameters which can be specified in an input Configuration File.

The output is a vector line and metadata associated with the image acquisition and the processing configuration used.

2.1.1 Pre-requisite

SAR images need to be radiometrically calibrated and orthorectified.

2.2 Algorithm Input

The input files needed are listed in Table 1:

Mission	Product type
Sentinel 1A and 1B	S1_IW_GRD -> Interferometric Wide Swath Ground Range Detected[14]]
Envisat	ASA_IMP_1P -> ASAR Image Mode Precision Image[15]
ERS	SAR_IMP_1P -> SAR Precision Image product[16]

Table 1. Input missions and product types

2.3 Theoretical Description of the models in background of the procedure

2.3.1 Physical Description

Unlike passive optical sensors that require the sun's illumination, an active SAR instrument transmits its own microwave signal to illuminate the Earth's surface at an angle. SAR actively transmits microwave signals towards the Earth and receives a portion of transmitted energy as backscatter from the ground. The returned backscatter echo of the scene is received by the instrument's antenna a short time later at a slightly different location, as the satellite travels along its orbit. The brightness amplitude of the returned signal, along with its phase information, is recorded to construct an image of the scene.

The frequency of the incident radiation determines:

- the penetration depth of the waves for the target imaged;

[14] Sentinel 1 products link

[15] Envisat ASAR Product Handbook link

[16] ERS SAR link

- the relative roughness of the surface considered.

The scattering examples for X and L band over a flooded and non-flooded area are shown in Figure 9

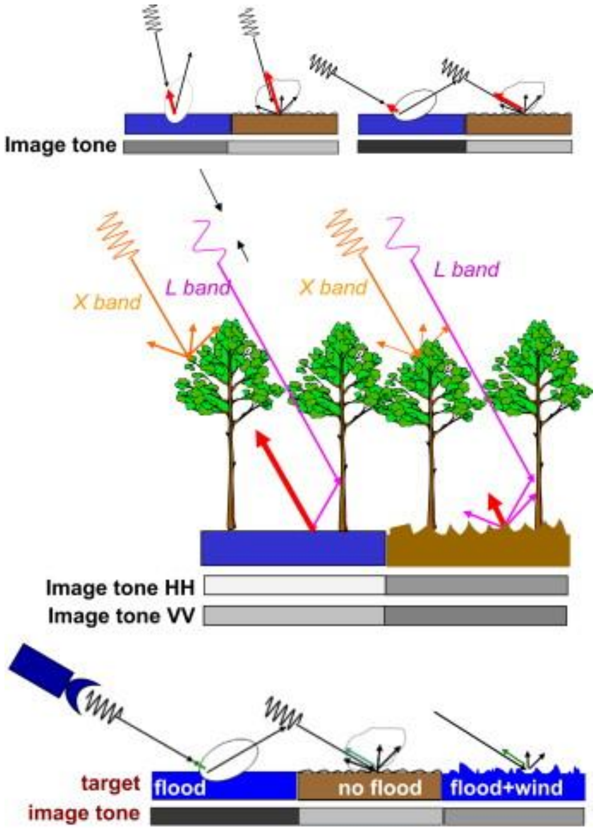

Figure 9. A Scattering mechanisms determining the radar signature of flooded terrain. Upper panel: flat water surface (blue) compared to rough soil (brown). Middle panel: flat water (blue) beneath vegetation compared to vegetated soil (brown). Bottom panel: flat water compared to water roughened by wind and to rough soil. Pierdicca[17] (2013)

The SAR instrument provides radar backscatter measurements influenced by the terrain structure and surface roughness. Generally, the more roughness or structure on the ground, the greater the backscatter. Rough surfaces will scatter the energy and return a significant amount back to the antenna resulting in a bright feature. Water bodies tend to be relatively smooth, except in the case of wind-stress or high waves travelling perpendicular to the satellite track, with most of the energy

---

[17] Pierdicca, N., Pulvirenti, L., Chini, M., Guerriero, L., & Candela, L. (2013). Observing floods from space: Experience gained from COSMO-SkyMed observations. Acta Astronautica, 84, 122–133. doi:10.1016/j.actaastro.2012.10.034

being reflected away from the radar and only a slight backscatter towards the radar. On the contrary, land surfaces tend to have a higher roughness.

In the microwave region, this difference between respective properties of land and water can be extremely useful for such applications as flood extent measurement or coastal zones erosion.

The SAR's ability to delineate the land/water boundary and to map geomorphological features is dependent on the incident angle (Leconte and Pultz [18] 1991, Lewis [19] et al. 1998). In low relief environments, small incidence angles (10 to 25 degrees from vertical) will produce the maximum relief enhancement, but larger incidence angles (25 to 59 degrees) will also result in acceptable terrain rendition by increasing the terrain textural contrasts (Singhroy [20] and Saint-Jean 1999). Normally, the coastline delineation is best achieved using large incidence angle (25-59 degrees) due to the high contrast in radar return from land (surface and volume scattering mechanisms) and water (specular reflection mechanism). However, surface variations and flooded vegetation are best-characterized using small incidence angle (25-40 degrees)[21].

2.3.2 Mathematical Description and calculation procedures

The processing chain consists of four main processes: Enhancement, Segmentation, Healing, and Vectorisation.

- **Enhancement**

---

[18] LECONTE R AND PULTZ TJ. 1991. Evaluations of the potential of RADARSAT for flood mapping using simulated satellite imagery. Can J Remote Sens 17: 241-249

[19] LEWIS AJ, HENDERSON FM AND HOLCOMB DW. 1998. Radar fundamentals: the geoscience perspective. In: HENDERSON FM AND LEWIS AJ. (Ed.), Principles & Applications of Imaging Radar. Manual of Remote Sensing, 3rd ed. New York: John Willey, p. 131-180.

[20] SINGHROY V AND SAINT-JEAN R. 1999. Effects of relief on the selection of RADARSAT-1 incidence angle for geological applications. Can J Remote Sens 25: 211-217.

[21] Souza-Filho, Pedro WM, and Waldir R. Paradella. "Use of synthetic aperture radar for recognition of Coastal Geomorphological Features, land-use assessment and shoreline changes in Bragança coast, Pará, Northern Brazil." Anais da Academia Brasileira de Ciências 75.3 (2003): 341-356.

In order to improve the results of the binary segmentation, the SAR image can first be enhanced. These enhancements are applied in order to compensate for expected characteristics of the SAR image such as salt-and-pepper thermal noise and illumination gradients caused by antenna beam roll-off. An example of the effect of applying the enhancement methods to a Sentinel-1 GRD image can be seen in Figure 10.

The methods that can be applied to enhance the image include roll-off compensation, Doerry [22] (2006), wavelet decomposition denoisisng, Achim[23] (2003), Lee and Sigma filters, Lee[24] (2008), and anisotropic diffusion, Yu[25] (2002). Each of these methods may be enabled or disabled separately via corresponding parameters in the Configuration File.

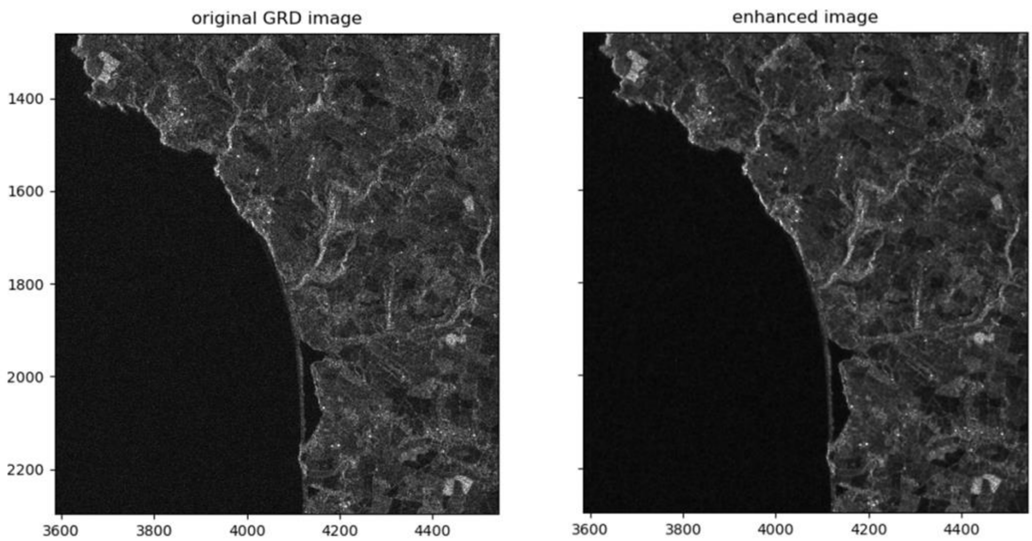

Figure 10. A Sentinel-1 GRD SAR image of Start Bay, before and after the application of enhancement routines

---

[22] Doerry, Armin Walter. Automatic compensation of antenna beam roll-off in SAR images. No. SAND2006-2632. Sandia National Laboratories, 2006

[23] Achim, Alin, Panagiotis Tsakalides, and Anastasios Bezerianos. "SAR image denoising via Bayesian wavelet shrinkage based on heavy-tailed modeling." IEEE Transactions on Geoscience and Remote Sensing 41.8 (2003): 1773-1784.

[24] Lee, Jong-Sen, et al. "Improved sigma filter for speckle filtering of SAR imagery." IEEE Transactions on Geoscience and Remote Sensing 47.1 (2008): 202-213.

[25] Yu, Yongjian, and Scott T. Acton. "Speckle reducing anisotropic diffusion." IEEE Transactions on image processing 11.11 (2002): 1260-1270.

- **Segmentation**

The SAR Waterline Processor produces an initial estimation of the land-sea boundary in the form a binary raster. This is produced by a simple threshold of the enhanced SAR image. The SAR Waterline Processor implements a range of methods for calculating the appropriate intensity value of the threshold, including Kittler [26] (1986) and Otsu[27] (1979) dynamic thresholds. The desired method can be specified in the Configuration File.

- **Healing**

Once the initial estimation of the waterline has been found by the segmentation algorithm, the binary raster that has been produced is then improved by applying a range of binary morphology operations, J. Serra[28] (1993). The purpose of this process is to eliminate erroneous features that might appear in the initial estimation of the waterline. An example of the effect of applying the healing methods can be seen in Figure 11.

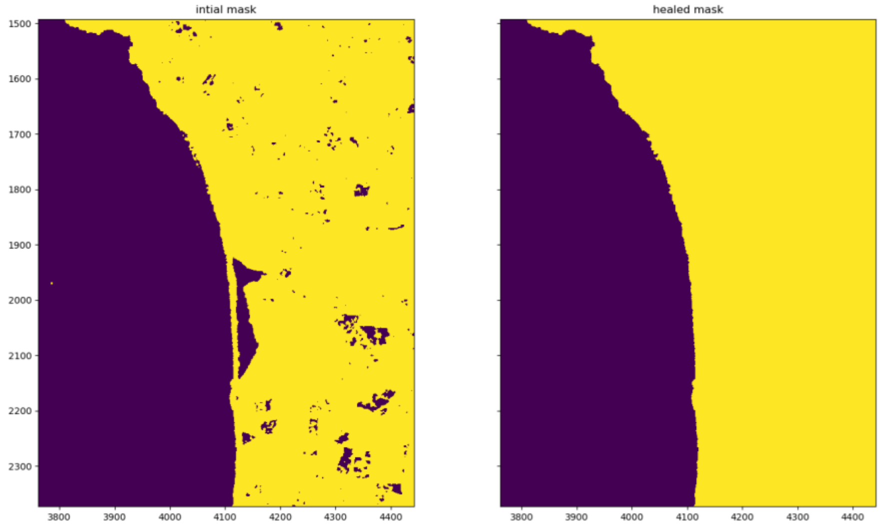

Figure 11. A binary raster image of Start Bay, before and after the application of healing methods.

[26] Kittler, Josef, and John Illingworth. "Minimum error thresholding." Pattern recognition 19.1 (1986): 41-47.

[27] Otsu, Nobuyuki. "A threshold selection method from gray-level histograms." IEEE transactions on systems, man, and cybernetics 9.1 (1979): 62-66.

[28] Serra, Jean. Image analysis and mathematical morphology. Academic Press, Inc., 1983.

The first method applied in the Healing process is binary opening. This is used to remove small foreground features which may be caused by bright reflections from waves or vessels. After this, a minimum size filter is applied, in which contiguous foreground areas of less than the number of pixels specified in the corresponding configuration parameter are removed from the raster. Lastly, holes within foreground features are filled.

- **Vectorisation**

The last step of the SAR Waterline Processor is to produce a waterline vector from the healed binary raster. This is found using the Marching Squares algorithm, Maple[29] (2003). The SAR Waterline Processor implements an option to blur the edges of the binary raster before the application of the Marching Squares algorithm, which enables smoothing of the vector to sub-pixel precision and reduces aliasing effects. The waterline vector may then be exported in either a KML or GeoJSON format file. An example of the waterline vector produced is shown in Figure 12.

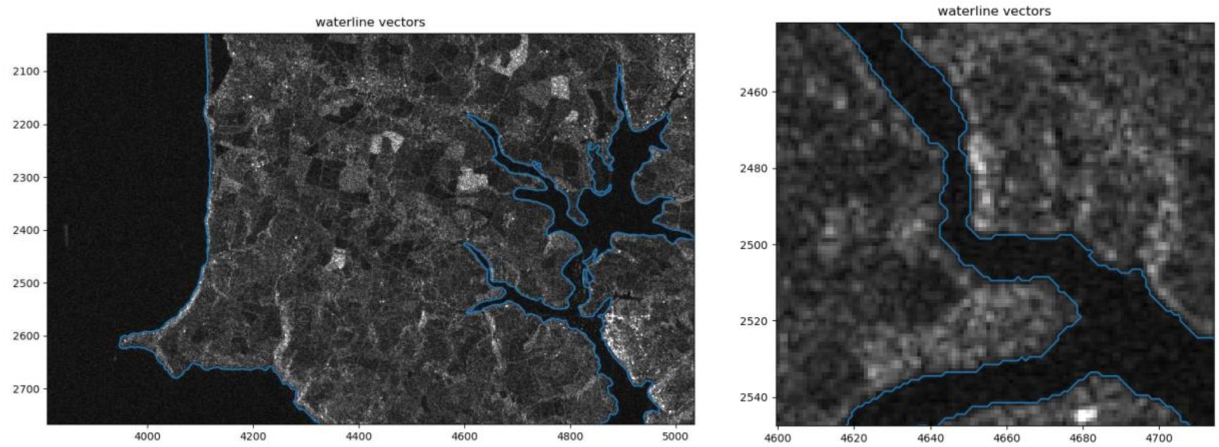

Figure 12. The calculated waterline vector overlaid on the Sentinel-1 GRD image from which it was produced.

[29] Maple, Carsten. "Geometric design and space planning using the marching squares and marching cube algorithms." 2003 International Conference on Geometric Modelling and Graphics, 2003. Proceedings. IEEE, 2003

2.3.3 *Acceptance of the Models*

The different options provided by this this processor have given good results over different particular locations in different publications, listed in Table 2.

Segmentation Method	Publications
Otsu	1. Bruno, Maria Francesca, et al. "Coastal observation through Cosmo-SkyMed high-resolution SAR images." *Journal of Coastal Research* 75.sp1 (2016): 795-800. 2. Ding, Xianwen, and Xiaofeng Li. "Coastline detection in SAR images using multiscale normalized cut segmentation." *2014 IEEE Geoscience and Remote Sensing Symposium*. IEEE, 2014. 3. Modava, Mohammad, and Gholamreza Akbarizadeh. "Coastline extraction from SAR images using spatial fuzzy clustering and the active contour method." *International journal of remote sensing* 38.2 (2017): 355-370. 4. Liu, Zhongling, et al. "A novel region-merging approach for coastline extraction from sentinel-1A IW mode SAR imagery." *IEEE Geoscience and remote sensing letters* 13.3 (2016): 324-328.
Kittler	1. Crawford, Melba M., et al. "Fusion of airborne polarimetric and interferometric SAR for classification of coastal environments." *IEEE Transactions on Geoscience and Remote Sensing* 37.3 (1999): 1306-1315. 2. Martinis, Sandro, et al. "Comparing four operational SAR-based water and flood detection approaches." *International Journal of Remote Sensing* 36.13 (2015): 3519-3543. 3. Ricard, Michael R., et al. "Multisensor classification of wetland environments using airborne multispectral and SAR data." *IGARSS'97. 1997 IEEE International Geoscience and Remote Sensing Symposium Proceedings. Remote Sensing-A Scientific Vision for Sustainable Development*. Vol. 2. IEEE, 1997. 4. Bovolo, Francesca, and Lorenzo Bruzzone. "A split-based approach to unsupervised change detection in large-size SAR images." *Image and Signal Processing for Remote Sensing XII*. Vol. 6365. International Society for Optics and Photonics, 2006.

Table 2. Segmentation methods and related publications

Additionally, there are examples with different enhancement methods as is listed in Table 3.

Enhancement Method	Publications
Sigma	1. Lee, Jong-Sen, et al. "Improved sigma filter for speckle filtering of SAR imagery." *IEEE Transactions on Geoscience and Remote Sensing* 47.1 (2008): 202-213. 2. Lee, Jong-Sen, et al. "Polarimetric SAR speckle filtering and the extended sigma filter." *IEEE Transactions on geoscience and remote sensing* 53.3 (2014): 1150-1160.
Lee	1. Rathore, Manvender Singh. *Statistical analysis of Synthetic Aperture Radar (SAR) image speckle*. Diss. 2014. 2. Qiu, Fang, et al. "Speckle noise reduction in SAR imagery using a local adaptive median filter." *GIScience & Remote Sensing* 41.3 (2004): 244-266.
Anisotropic diffusion	1. Liu, Hongxing, and Kenneth C. Jezek. "A complete high-resolution coastline of Antarctica extracted from orthorectified Radarsat SAR imagery." *Photogrammetric Engineering & Remote Sensing* 70.5 (2004): 605-616. 2. Gupta, Anurag, Anubhav Tripathi, and Vikrant Bhateja. "Despeckling of SAR images via

	an improved anisotropic diffusion algorithm." *Proceedings of the International Conference on Frontiers of Intelligent Computing: Theory and Applications (FICTA)*. Springer, Berlin, Heidelberg, 2013.

Table 3. Enhancement methods and related publications

The size of both Lee and Sigma filters needs to be specified as an input parameter.

Frost and Kuan methods have been preliminary withdrawn but can be option to be implemented in future releases of this processor.

The implemented anisotropic diffusion method has 3 different input parameters (gamma, kappa and the number of iterations). The ones selected by Liu et al in the publication are gamma= 0.25, kappa=8, number of iterations=5.

Regarding the morphology operations, the size of the disk has been set to 5 pixels.

2.3.4 Error estimation

Possible error may be classified in different categories, errors from the instrument, the satellite sensors, errors from product pre-processing like co-registration or geometric and radiometric correction, and errors from the waterline extraction model. Systematic colocation biases can be detected and corrected after the validation is performed.

The signal to noise ratio (SNR) is a key parameter of satellite sensors, it quantifies how much the signal has been corrupted by noise. It characterizes the actual information content in an image – radiometric resolution. The radiometric resolution of an imaging system describes its ability to discriminate very slight differences in energy.

2.4 Algorithm output

Proxy based and datum-based shorelines will be delivered with their metadata. Lines will be delivered in vector format and will be compatible with common GIS software.

2.4.1 Product content

The output of the SAR waterline is a vector line file (geojson or kml format) and a csv file with the following metadata:

- configuration settings
- mission
- date + time*
- input filename
- polarisation mode*
- orbit (number) information*
- sense* (ascending/descending)
- intermediate parameters:
  - threshold level
  - image mean intensity
  - water mean intensity
  - land mean intensity
- configuration settings that are used

*parameters that are read from the input auxiliary information provided as a separated XML or included in the headers of the image file.

2.4.2 Product Management

Waterline products will be organized in different folders according to the study area. For each area partners will access the waterline with all metadata

2.5 Algorithm Performance Estimates

2.5.1 Test specification

Tests will be conducted to evaluate the ability of the processor to extract a continuous waterline. Several tests need to be conducted for different locations to test the process accuracy in different environments.

2.5.2 Test Datasets

First test within a ROI in Start. The processor extracted WL from a S1B image from March 23th, 2019.

2.5.3 Validation

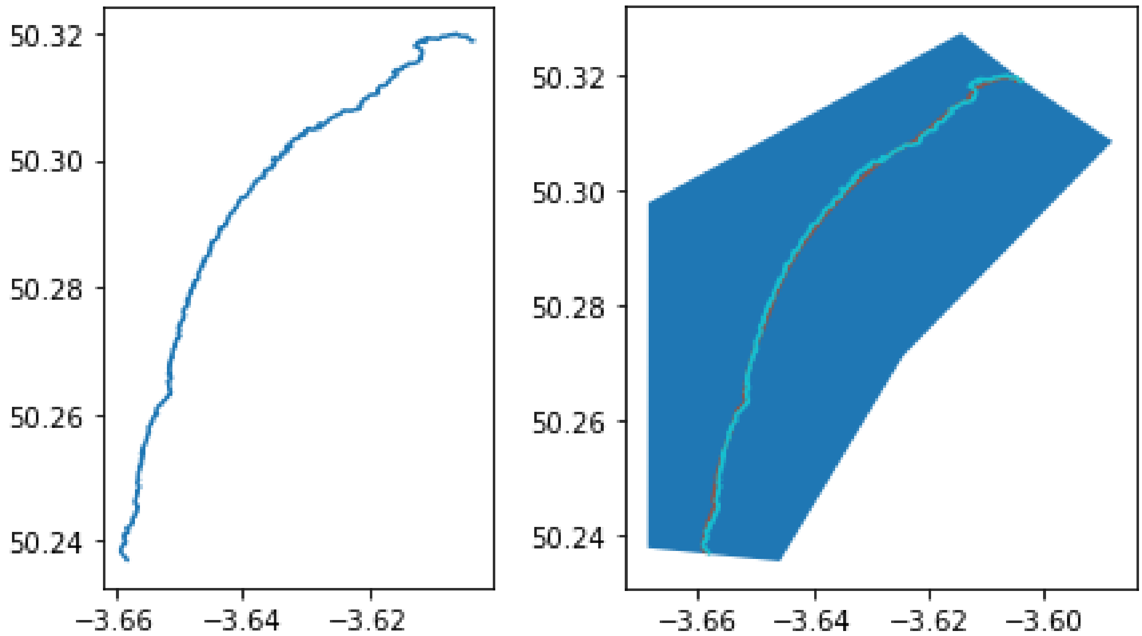

Figure 13. Right: Waterline retrieved from S1B over the Start Bay area the 23th of May 2019, image filename: S1B_IW_GRDH_1SDV_20190323T063105_20190323T063130_015478_01CFE3_BD7C. Left: Comparison between the waterline retrieved from S1B and the validation one retrieved from S2A

2.5.4 Practical Considerations

On Figure 13 we can see the waterline from a S1B is compared with another reference waterline. The area between them can be computed and used as a similarity indicator. We did the analysis of 2 years of S1 images from Barcelona and Start Bay pilot sites and classified the waterlines retrieved between success, when the similarity indicator was higher that 75%; fail, when the similarity was lower than 35% and mitigate for the rest of the cases. We did it using different options of the processing chain (Otsu or Kittler thresholding, different lee and sigma filter sizes, anisotropic diffusion on/off, subpixeling on/off), all the available polarisations and geometries.

The results for the 13 different configuration options are shown in Figure 14.

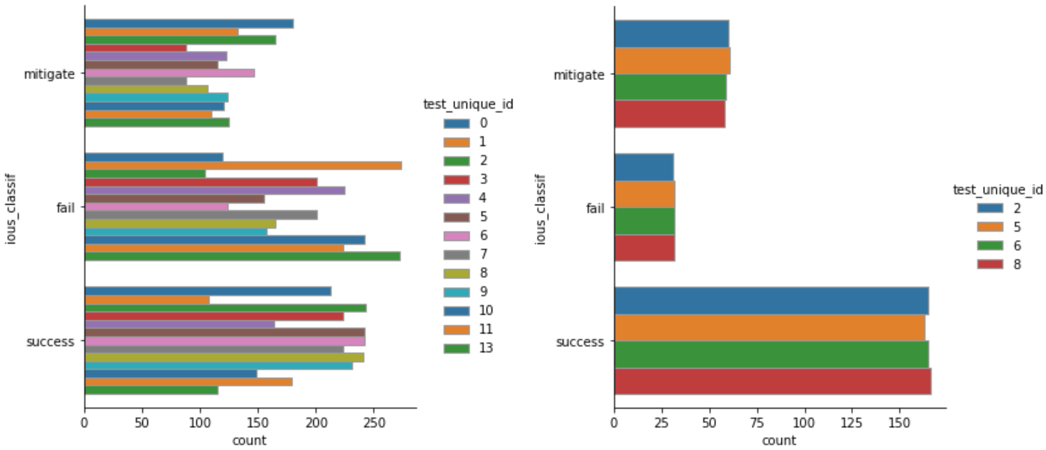

Figure 14. Number of successful, fail and mitigate results for each of the initial 13 configurations (left) and the results for the selected configurations to be further validated (right).

By checking the orbit sense (shown in Figure 15), we can see that there are more fail cases when the orbit is descending. This is because the geometry in both Barcelona and start bay areas is very similar (Land in the North-North West and Water in the South-South East).

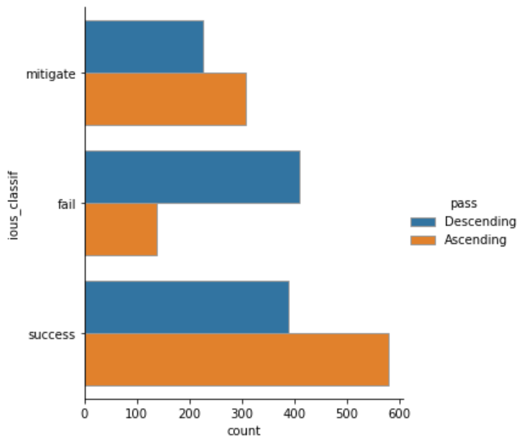

Figure 15. Number of successful, fail and mitigate results between ascending and descending acquisitions.

Finally, and a bit more tricky, if we have a look at the mean water, land, and overall image intensities (shown in Figure 16) we can also identify some areas of good performances. If we pay attention to the top right and bottom left subplots, it is clear that the success results are quite well separated from the other two groups.

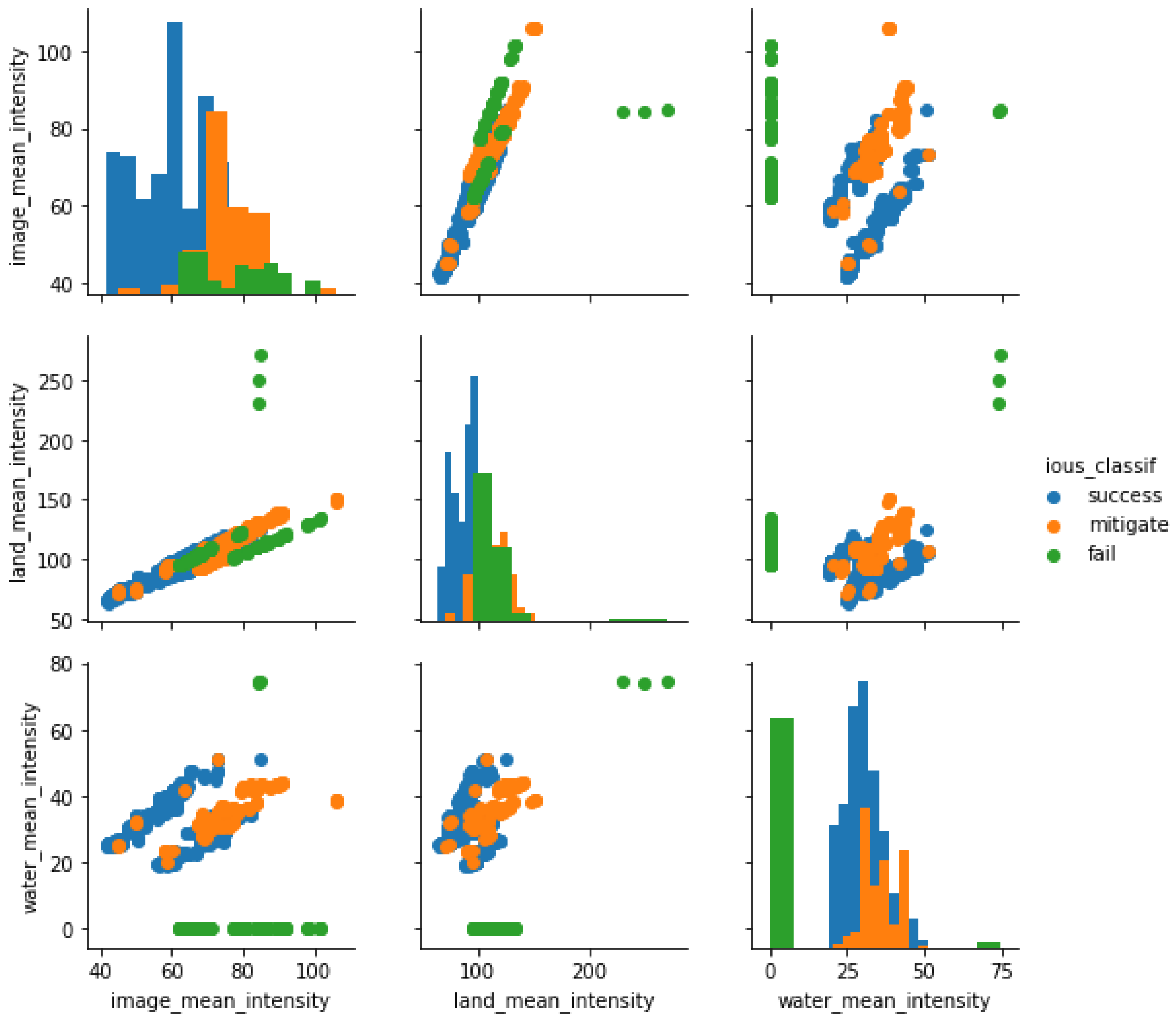

Figure 16. Location of the successful, fail and mitigate results depending on the land, water and overall image mean intensities.

2.6 Products Validation

2.6.1 Test specifications

Validation tests will be conducted to evaluate the accuracy of the extracted WL. It will mainly be a comparison of the WL position with some visual identification of the WL on VHR data (VHR satellite imagery, LiDAR surveys, etc.). From this comparison we will calculate the distance between extracted lines and the visual boundary between the different areas.

2.6.2 Test Datasets

Data from the partners and in-situ surveys are needed to run tests for each location sites.

2.6.3 Validation

Will be completed in version 2, following result from feasibility study.

2.6.4 Practical Considerations

3 Conclusion

3.1 Assessment of limitations

The limitations identified to date in the feasibility phase stem from the method used: edge detection. After a binary classification of the image to either land or water, the algorithm creates a line at the boundary of the two. However, this line is not always continuous, and the boundary classification is not always correct. Therefore, the resulting discontinuities and false edges pose problems for being able to define the final waterline product in certain cases.

In some cases, the waterline can be wrongly estimating the boundary between wet and dry sand in the case of very flat beaches and in low tide events.

Additionally, some human made constructions or metal structures can appear in the SAR image as bright targets shadowing the real waterline boundary an being unable to retrieve it properly.

3.2 Mitigation

Some intermediate parameters have been included in the output waterlines in order to better understand if bad weather conditions can be filtered out. The mean water and mean land intensities computed during the segmentation process can be used to filter out waterlines when the water and land backscatter is very similar.

Regarding the human made constructions, the location of groynes (sea defences) and piers is well known by the user community and can be incorporated as an input in the algorithm to avoid computing the waterline around them.

4 References

5 Appendix

End of Document